Pure Appl. Geophys. 173 (2016), 369–387

DOI 10.1007/s00024-015-1226-3

Pure and Applied Geophysics

Real-Time Assessment of the 16 September 2015 Chile Tsunami and Implications for Near-Field Forecast

Liujuan Tang,[1,2] Vasily V. Titov,[2] Christopher Moore,[2] and Yong Wei[1,2]

Abstract—The magnitude 8.3 earthquake in central Chile on 16 September 2015 and the resulting tsunami severely affected the region, with 15 deaths (Onemi in Monitoreo por sismo de mayor intensidad. (In Spanish) [Available at: http://www.onemi.cl/alerta/se-declara-alerta-roja-por-sismo-de-mayor-intensidad-y-alarma-de-tsunami/], 2015), over one million evacuated, and flooding in nearby coastal cities. We present our real-time assessment of the 2015 Chile tsunami using the Short-term Inundation Forecasting for Tsunamis system, and post-event analyses with local community models in Chile. We evaluate three real-time tsunami sources, which were inverted at the time that the first quarter-, half-, and full-wave passed the first tsunameter (DART 32402, located approximately 580 km north–northwest of the epicenter), respectively. Measurement comparisons from 26 deep-ocean tsunameters and 38 coastal tide stations show that good model accuracies are achieved for all three sources, particularly for the local sites that recorded the most destructive waves. The study highlights the forecast speed, time and accuracy dependence, and their implications for the local forecast capability. Our analyses suggest that the tsunami's main origination area is about 100–200 km long and 100 km wide, to the north of the earthquake epicenter along the trench and the total estimated tsunami wave energy is 7.9×10^{13} J (with 13 % uncertainty). The study provides important guidelines for the earliest reliable estimate of tsunami energy and local forecasts. They can be obtained with the first quarter-wave of tsunameter recording. These results are also confirmed by a forecast analysis of the 2011 Japan tsunami. Furthermore, we find that the first half-wave tsunameter data are sufficient to accurately forecast the 2015 Chile tsunami, due to the specific orientation between the nearest tsunameter and the source. The study also suggests expanding the operational use of the local community models in real time, and demonstrates the applicability of the model results for "all-clear" evaluations, search and rescue operations, and near-real-time mitigation planning in both near and far fields.

Key words: The 2015 Chile tsunami, tsunami forecast, tsunami source, tsunami energy, near-field forecast, numerical modeling.

1. Introduction

On the evening of 16 September 2015 at 19:54:33 local time (22:54:33 GMT), a moment magnitude (M_w) 8.3 earthquake occurred on the South American subduction zone, the plate boundary between Nazca and South America plates. According to the US Geological Survey (USGS), the epicenter of the earthquake was located at 31.57°S and 71.67°W, 48 km west of Illapel, in the region of Coquimbo, central Chile. Estimates of the earthquake magnitude varied from M_w 7.9 to 8.3 during the first 30 min after the earthquake (PTWC, TSUNAMI MESSAGE NUMBER 1–2) (Fig. 1). Later Centroid-Moment-Tensor analysis indicated a magnitude of M_w 8.2 (GCMT) or M_w 8.3 (USGS) (http://earthquake.usgs.gov/earthquakes/eventpage/us20003k7a#scientific_summary).

The earthquake generated a destructive tsunami—yet another in Chile's long history of large tsunamigenic events (Fujii and Satake 2013; Ye *et al.* 2015). The resulting tsunami produced waves of 4.6 m positive amplitude at Coquimbo's sea-level station, and flooding in this harbor town and the nearby cities of Tongoy and Concón. In Coquimbo, the flooding spread to many parts of the city, causing extensive damage to the port, the fishing wharf, and much of downtown (Bonnefoy and Romero 2015). Flooding in Tongoy was extensive, destroying a preschool, a police station, and part of a health clinic. Run-up of about 10 m was reported near epicenter areas (http://

This paper is part of the article collection on "Illapel, Chile, Earthquake on September 16th, 2015".

Electronic supplementary material The online version of this article (doi:10.1007/s00024-015-1226-3) contains supplementary material, which is available to authorized users.

[1] Joint Institute for the Study of the Atmosphere and Ocean (JISAO), University of Washington, Box 355672, Seattle, WA 98105, USA.

[2] NOAA Center for Tsunami Research, Pacific Marine Environmental Laboratory, National Oceanic and Atmospheric Administration, 7600 Sand Point Way NE, Seattle, WA 98115, USA. E-mail: vasily.titov@noaa.gov

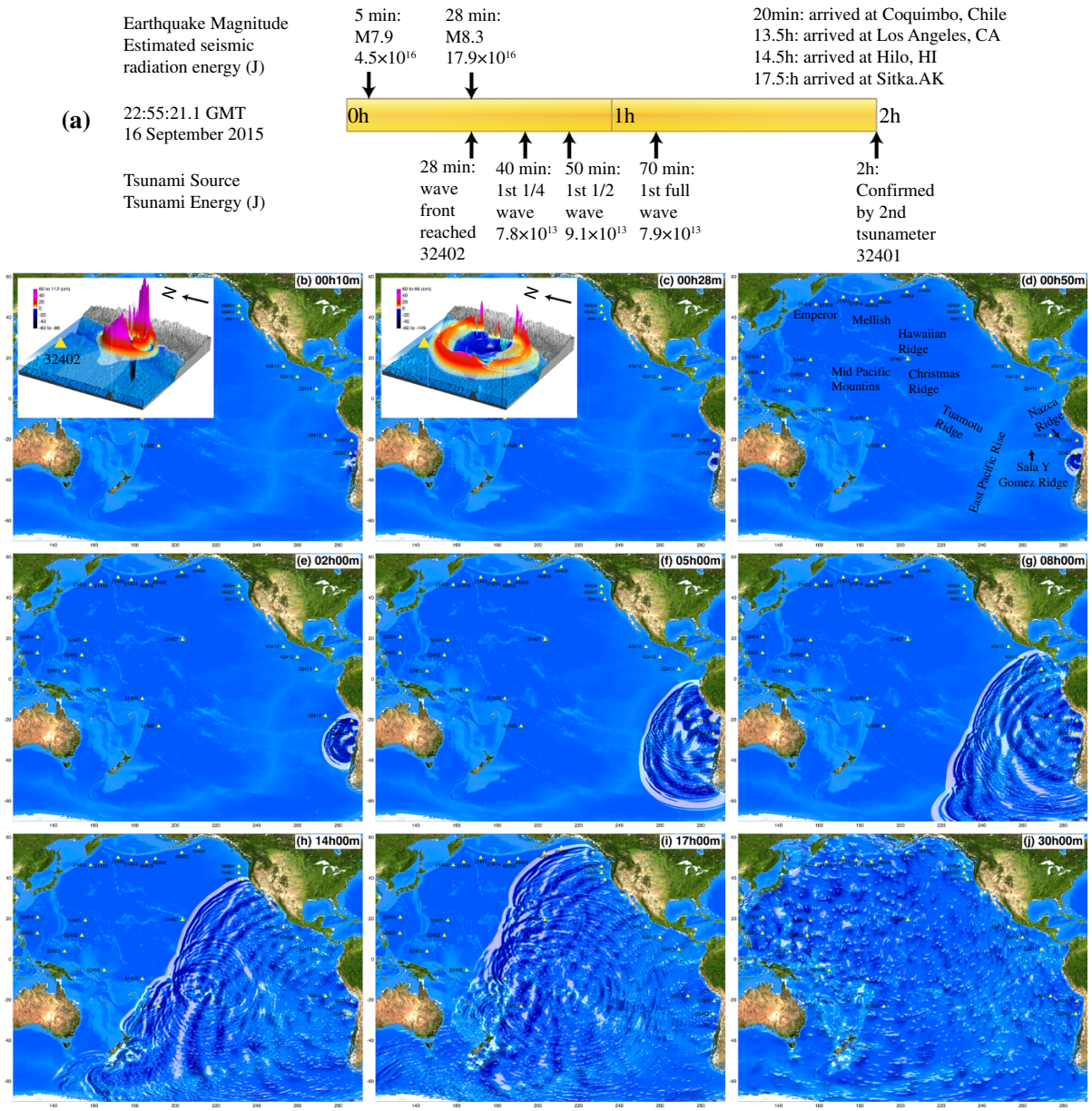

Figure 1
a Timeline for assessment of the September 16, 2015 Chile earthquake and tsunami. **b–j** Snapshots of modeled tsunami wave patterns in deep ocean during 30 h of propagation. The *insets* in **b** and **c** show close-up of modeled tsunami amplitudes in cm

www.24horas.cl/nacional/especialistas-registran-olas-de-hasta-10-metros-en-la-region-de-coquimbo-1794582). Chile's national emergency service ordered the immediate evacuation of the mainland coast, as well as Easter Island and the archipelago of Juan Fernández. An unprecedented number of people evacuated coastal areas, heeding tsunami warnings or as self-evacuation. Over one million residents reportedly moved to higher ground immediately after the earthquake, which amounted to virtually the entire coastal population of the country (about 18 million residents). This mass evacuation clearly prevented a higher death toll from the intense tsunami inundation, which left clear signs of violent flooding in populated areas, though the vast majority of evacuation occurred from outside of

flooded zones. At the time of the publication, 8 of the 15 deaths reported for this event have been attributed to the tsunami (ONEMI 2015).

This was Chile's third massive quake in 5 years and the most recent in a long history of tsunamis and earthquakes in this very seismically active part of the world. The 27 February 2010 earthquake (M_w 8.8) in southern Chile killed 525 people, 124 of them due to tsunami flooding (FRITZ *et al.* 2011). Since then, the Chilean government has implemented sweeping changes in their national tsunami warning procedures and tsunami hazard mitigation measures. The results of those changes and the increased awareness of the population were evident during the next flooding tsunami, the 1 April 2014 Iquique Chile tsunami (M_w 8.2), which created a massive evacuation with no tsunami casualties, and again during this event. Chile also holds the record of the strongest instrumentally recorded earthquake in history, the 22 May 1960 Chile earthquake, with a moment magnitude estimate of M_w 9.5 (KANAMORI 1977). Tremendous local and global impacts of the 1960 tsunami led to the establishment of local and global services to deal with such catastrophes: UNESCO's Pacific-wide Tsunami Warning System and the local Chilean Emergency Committee (now the National Office of Emergency of the Interior Ministry, or ONEMI). Both continue to operate at present.

The 2015 Chile tsunami may be the first large-scale flooding tsunami to inundate highly populated areas within minutes from tsunami generation while mass casualties were largely avoided. Our study considers lessons learned from this successful example of early tsunami warning application and its implications for the local tsunami forecast problem. Our real-time assessment for the 2015 event was based on deep-ocean measurements from the tsunameter station DART 32402, operated by the Hydrographic and Oceanographic Service of the Chilean Navy (SHOA). This station is only 28 min of propagation time away from the tsunami source, which makes it essentially a near-field tsunameter. In addition, DART 32402 is advantageously positioned relative to the 2015 tsunami source. As will be discussed in Sect. 5, the difference in tsunami travel time (or travel distance) from adjacent source units is relatively significant. This separation allows for accurate determination of the source location. In contrast, the 2010 Chile tsunami (M_w 8.8) was first recorded at a tsunameter 3 h after the earthquake, making those essentially far-field measurements (http://nctr.pmel.noaa.gov/chile20100227/). The 2014 Iquique tsunami forecast (http://nctr.pmel.noaa.gov/chile20140401/) was based on the near-field tsunameter measurements of DART 32401 (only 20 min of propagation time from the source). However, the tsunami travel path from the 2014 source to DART 32401 was nearly perpendicular to the trench. This made it alone insufficient to determine the tsunami source due to the similarity in travel time from adjacent unit sources. Therefore, the 2015 Chile tsunami, especially in comparison with previous Chilean events, provides a unique opportunity to investigate the minimum amount of data required to produce a reliable forecast in the shortest possible time.

Section 2 of this article briefly describes the forecast method. Section 3 presents the assessment of the 2015 Chile tsunami in real time, including the tsunami sources and energy. Section 4 discusses coastal impact and summarizes the model accuracy. Section 5 discusses the guidelines and implications for fast and reliable forecast application. A forecast analysis of the 2011 Japan tsunami is also included in this section to illustrate the forecast system performance when the nearest tsunameter is not optimally located for inversion purpose. Conclusion and future work are provided in Sect. 6.

2. *Tsunami Forecast Method*

The generation of an earthquake-induced tsunami is modeled as the instantaneous rupture of a single rectangular fault plane characterized by pre-defined parameters describing the location, orientation and rupture of the plane (GUSIAKOV 1978; OKADA 1985). In this study, we refer to a propagation scenario generated by a typical M_w 7.5 subduction earthquake from a particular location, with predefined parameters of length = 100 km, width = 50 km, slip = 1 m, and rake angle = 90° as a *unit source* (Fig. S1). Other parameters, including depth, dip angle, and strike angle, are location-specific. Wave dynamics of tsunami propagation in deep-ocean are assumed to be

linear (Mei *et al.* 2005; Liu 2009). Hence a propagation scenario can be constructed as a superposition of unit sources.

Titov *et al.* (1999) has established that only few source parameters are critical to characterize far-field tsunamis, mainly the location and the magnitude. Other parameters have secondary influence and can be predefined for forecast purposes. Tang *et al.* (2012) show that the source location and the propagating wave energy are the two most important source characteristics for predicting tsunami flooding impacts in both far- and near-fields for the 2011 Great Japan Tsunami.

Tsunami source energy can be quantified in real time by measuring the tsunami wave energy spreading from the source in deep ocean, through the detection by tsunameters at more than 60 locations around the world oceans. Notwithstanding the details of earthquake processes generating tsunami waves, the inversion can determine a propagation scenario (i.e. a source scenario) that gives the best fit to tsunameter data. Therefore, this source scenario provides the best estimate of the tsunami source energy transferred by tsunami waves. More details on computing the tsunami energy are provided by Tang *et al.* (2012). Percival *et al.* (2011) describes the inversion technique for identifying the tsunami source using tsunameter data and pre-computed source units.

The tsunami research group (now known as NOAA Center for Tsunami Research) of the US National Oceanic and Atmospheric Administration (NOAA) Pacific Marine Environmental Laboratory (PMEL) has been developing the tsunami forecast system since 1980s. The operational version of the forecast system has been implemented for use by the US Tsunami Warning Centers (TWCs) since 2013. The system (known as Short-term Inundation Forecast for Tsunamis, or SIFT) combines deep-ocean observations (Milburn *et al.* 1996) and numerical modeling technology (Titov *et al.* 2015). It integrates three key components: the tsunameter network, the propagation database, and high-resolution inundation forecast models (Titov *et al.* 2005; Titov 2009; Bernard and Titov 2015), which correspond to the three distinct stages of tsunami evaluation: generation, propagation, and coastal run-up. Together these components provide a full forecast capability. The system has been tested extensively in forecast and hindcast studies for more than 40 historical tsunamis (Titov *et al.* 2005; Titov 2009; Wei *et al.* 2008, 2013; Tang *et al.* 2008, 2009, 2012; Titov and Tang 2011, 2015; Bernard *et al.* 2014).

Presently, the first component of the forecast system, the tsunameter network, comprised 63 stations, and is globally owned by nine counties (Fig. S1) (González *et al.* 2005; Meinig *et al.* 2005; Spillane *et al.* 2008). The second component of the forecast system uses the Method of Splitting Tsunami (MOST) model, a suite of finite difference numerical codes based on the long-wave approximations (Titov and Synolakis 1998; Titov and Gonzalez 1997; Synolakis *et al.* 2008; Titov *et al.* 2015). MOST is used to compute the unit sources in the propagation database (Gica *et al.* 2008). Currently, the database has 1990 unit scenarios covering the most active subduction zones in the Pacific, Indian, and Atlantic Oceans (Fig. S1). The third component of the forecast system is a set of high-resolution, site-specific inundation forecast models built on the MOST model to simulate the nonlinear wave dynamics near shore (Tang *et al.* 2009; Titov *et al.* 2015). Each inundation model contains three telescoping grids with increasing resolution, covering regional, intermediate, and near shore areas (e.g., Fig. S2). Inundation forecast models have been developed for 75 US coastal communities (54 in the Pacific, 21 in the Atlantic/Caribbean). Sea-level stations, when available at these locations, have been used to validate forecast accuracy for over 40 past tsunamis (e.g., Tang *et al.* 2009).

During a real-time forecast assessment, a tsunami source (i.e., a propagation scenario) is obtained by identifying the combination of unit sources that gives the best fit to tsunameter data. This model scenario is pre-computed and directly available. This saves simulation time of basin-wide tsunami propagation. It also provides valid boundary conditions, a linear combination of time series of offshore wave heights and depth-averaged velocities, which ensure the accuracy of the coastal tsunami impact predictions.

We applied the described forecast procedure in real time during the 2015 Chile tsunami event as the tsunami was propagating toward warning points along the US coastlines. A total of 54 operational

tsunami flooding forecast models in the US were exercised, with coastal tide gauge data later available for 35 models for comparison. In addition, three flooding models were developed and run for the communities of Coquimbo, Valparaiso, and Talcahuano to evaluate model accuracy in near field, as the post-event analyses. Those community models were developed as part of the ComMIT (Community Modeling Interface for Tsunami) training for Chile (Titov *et al.* 2011).

3. Assessment of Tsunami Source and Energy in Real Time

Tsunami forecasting is a race against time. For most tsunamis, the closest coastline is likely to be affected by the first wave within half an hour after generation. Therefore, every minute counts during tsunami warning procedures, including the generation of the tsunami forecast. Historically, computation time has been one of the main problems for the operational tsunami forecast. However, recent developments of tsunami modeling and computer science have moved the main bottleneck of the forecast process from computation time toward data availability. The critical data for our forecast method come from tsunameters. Therefore, the forecast is available no sooner than the first tsunami wave crest over the first tsunameter location. The wave period of a typical tsunami averages at about 20–30 min. Hence, the data length after the first peak that is needed for accurate forecasting is a critical parameter for local warning procedures, since every additional data point adds minutes to the time of forecast availability. To investigate the potential for model-based local tsunami forecasting, we present our real-time assessment of the 2015 Chile tsunami, including the tsunami sources, energy, and details obtained by inverting the first quarter-, half-, and full-wave data available from the nearest tsunameter station.

Figure 1a shows the event timeline for the 2015 Chile tsunami. 28 min after the earthquake, the tsunami wave front reached the first tsunameter station, DART 32402, located approximately 580 km north–northwest of the epicenter. In 12 min, the first wave crest passed the station showing a maximum of 11 cm. Inverting this first quarter-wave in real time produced estimates of tsunami energy of 7.8×10^{13} J and a displaced water volume of 19 km^3. In another 10 min, the station recorded the first half-wave, giving an updated source to be determined with 9.1×10^{13} J tsunami energy and 25 km^3 displaced water volume. Twenty min later, i.e., 70 min after the earthquake, the station recorded the first full-wave. Inversion of the first full-wave indicated tsunami energy of 7.9×10^{13} J, which differs 2 and 13 % from the first and second estimates, respectively. These variations in tsunami energy estimates are relatively small, compared to the changes in order of magnitudes in seismic energy estimates. The displaced water volume for the third source is 26 km^3, less than 4 % difference from the half-wave source. The half- and full-wave sources give a better fit to the data at 32402, particularly for the overall wave period (Fig. 2.1). Table 1 summarizes the source coefficients along with the pre-defined parameters for the three tsunami sources. The initial ocean surface displacements reconstructed from the three sources are plotted in Fig. 3. The results indicate a major tsunami source area of 100–200 km long and 100 km wide (2–4 unit sources), mainly to the north of the earthquake epicenter along the trench.

We observe that none of the three sources reproduced the trough (−8.4 cm) measured near 0.9 h at station 32402 (Fig. 2.1). The wavelet analysis reveals that this trough has a very short peak period of 9 min, compared to the main peak periods of 31 and 61 min for the entire data time series (Fig. 4a2, a3). Several factors could potentially have caused this short period trough: the local fine bathymetric effect, noise embedded into the tsunameter signals, or a very small-scale tsunami source feature that was not captured by the unit source resolution. The spectrogram shows high-frequency components can be caused by the under-sampled seismic signals (1-min data rate) prior to the arrival of the first wave (Fig. 4a3). In addition, the propagation database has a spatial resolution of 4 arc min, which is approximately 6.3 km at 31.57°S in Chile along the E–W direction and 7.4 km along the N–S direction. The first half of the tsunami wave carries direct information from the source of the tsunami, while the following includes complex interaction of the wave with bathymetry and coastal features that may not be fully resolved with

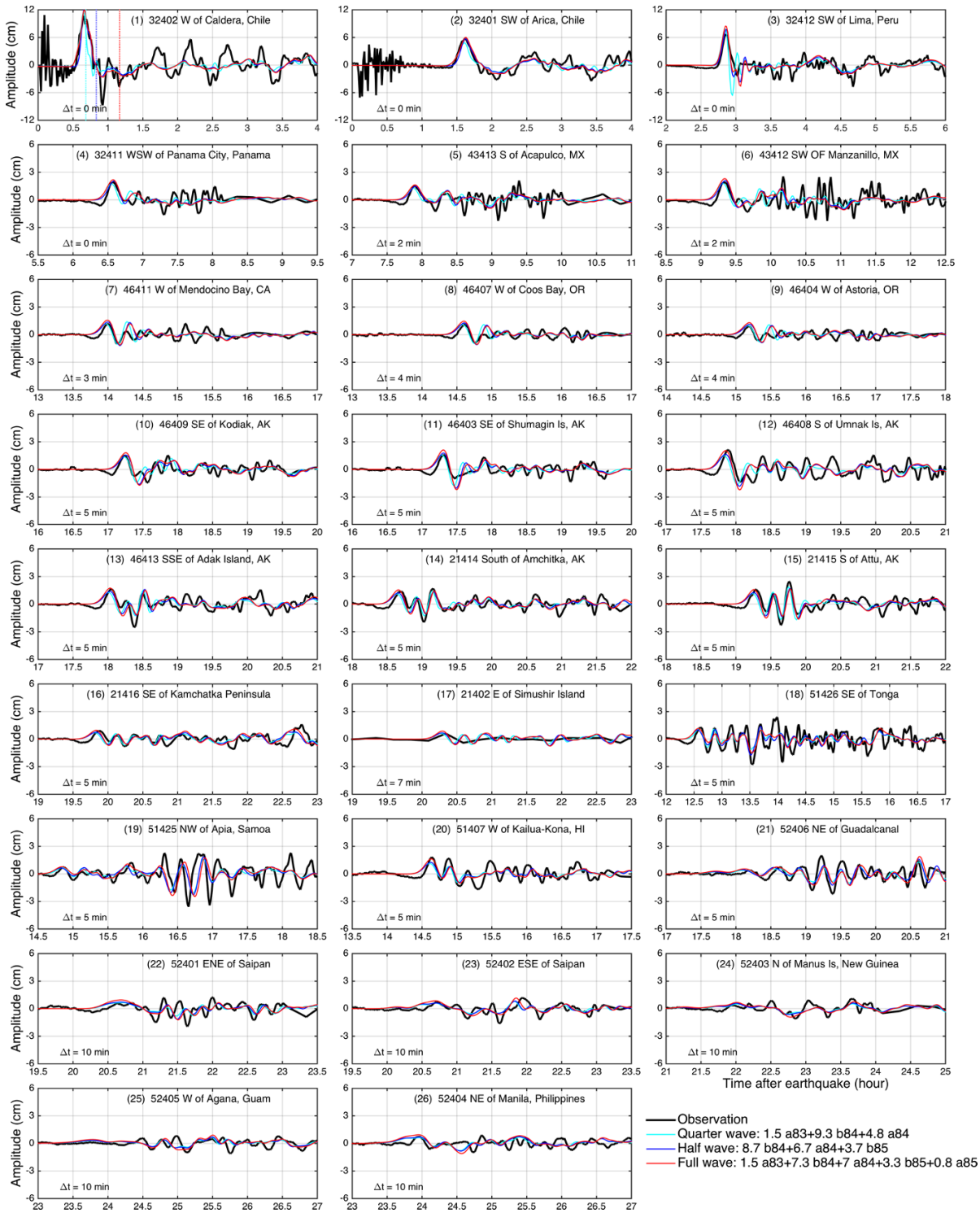
(1) 32402 W of Caldera, Chile
(2) 32401 SW of Arica, Chile
(3) 32412 SW of Lima, Peru
(4) 32411 WSW of Panama City, Panama
(5) 43413 S of Acapulco, MX
(6) 43412 SW OF Manzanillo, MX
(7) 46411 W of Mendocino Bay, CA
(8) 46407 W of Coos Bay, OR
(9) 46404 W of Astoria, OR
(10) 46409 SE of Kodiak, AK
(11) 46403 SE of Shumagin Is, AK
(12) 46408 S of Umnak Is, AK
(13) 46413 SSE of Adak Island, AK
(14) 21414 South of Amchitka, AK
(15) 21415 S of Attu, AK
(16) 21416 SE of Kamchatka Peninsula
(17) 21402 E of Simushir Island
(18) 51426 SE of Tonga
(19) 51425 NW of Apia, Samoa
(20) 51407 W of Kailua-Kona, HI
(21) 52406 NE of Guadalcanal
(22) 52401 ENE of Saipan
(23) 52402 ESE of Saipan
(24) 52403 N of Manus Is, New Guinea
(25) 52405 W of Agana, Guam
(26) 52404 NE of Manila, Philippines
Amplitude (cm)
Time after earthquake (hour)
Observation
Quarter wave: 1.5 a83+9.3 b84+4.8 a84
Half wave: 8.7 b84+6.7 a84+3.7 b85
Full wave: 1.5 a83+7.3 b84+7 a84+3.3 b85+0.8 a85

◀Figure 2
Comparisons between modeled amplitude time series and measurements at 26 tsunameter stations for the 2015 Chile tsunami. *Cyan*, *blue*, and *red lines* represent the three tsunami sources inverted from the first quarter-, half-, and full-wave at station 32402, respectively. The *dotted lines* in (1) indicate the time and the length of data used for inversion. A time delay of Δt minutes was applied to the model time series in each panel

the coarse propagation model. Therefore, the first half-wave contains information more relevant to the tsunami source and is less influenced by the fine, local bathymetry features.

This is further supported by the measurements at the second tsunameter station, DART 32401 located 1250 km north of the epicenter. Data were available 2 h after the earthquake. Both the half- and full-wave sources provide excellent forecast results at this station (Fig. 2.2). The two sources also show a better match with the recorded wave period at the third tsunameter station 32412 (Fig. 2.3). Note there are several flat data points after the first trough at the station. In addition, all three sources produced good predictions of tsunami amplitude at 25 other tsunameters throughout the Pacific (Fig. 2).

Table 1

Pre-defined parameters for tsunami source functions and the three tsunami sources inverted from the first quarter, half, and full-wave at station 32402 for the 2015 Chile tsunami in real time

Tsunami source functions[a] (pre-defined)						Tsunami source coefficients (obtained in real time)		
Name	Longitude (°E)	Latitude (°N)	Strike (°)	Dip (°)	Depth (km)	Station 32402		
						Quarter wave	Half wave	Full wave
a83	288.5944	−30.2923	14.81	5.36	11.96	1.5	–	1.5
b84	288.0163	−31.1351	8	3.8	5	9.3	8.7	7.3
a84	288.5223	−31.1639	14.9	3.8	11.96	4.8	6.7	7.0
b85	287.9635	−32.0223	8	2.55	5	–	3.7	3.3
a85	288.4748	−32.0416	15	2.55	11.96	–	–	0.8
Tsunami energy E_T (J)						7.8×10^{13}	9.1×10^{13}	7.9×10^{13}
Displaced water volume (km^3)						19	25	26

[a] All the tsunami source functions have three common source parameters, length 100 km, width 50 km and slip 1 m

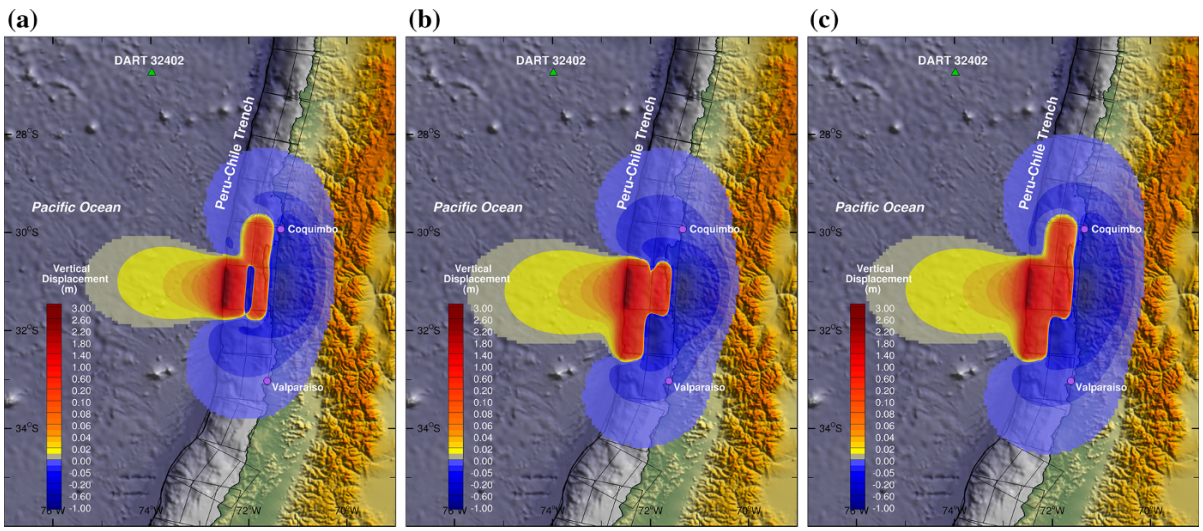

Figure 3
Initial ocean surface displacements reconstructed from tsunami sources inverted from the first (**a**) quarter-, (**b**) half-, and (**c**) full-wave recorded at station 32402 for the 2015 Chile tsunami

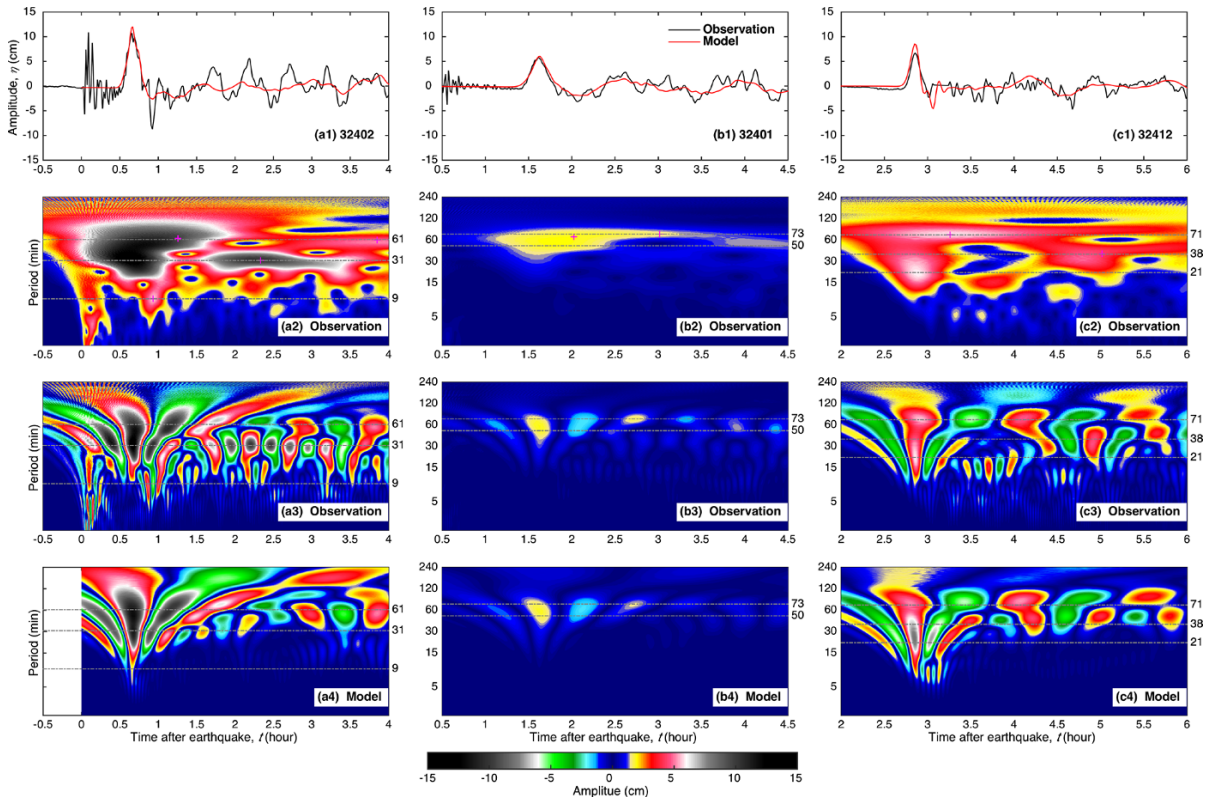

Figure 4

a1–c1 Time series of observed and modeled wave amplitudes at three nearest tsunameter stations for the 2015 Chile tsunami. **a2–c2** Wavelet-derived amplitude spectra of the observations show peak periods at the three stations, respectively. The real parts of the spectra are plotted in panels **a3–c3**. **a4–c4** The modeled tsunami waves reproduce the main frequency/period patterns of the observations well. Model results are obtained from the full-wave source

4. *Coastal Impacts and Model Accuracy*

The 2015 Chile tsunami was recorded at coastal sea-level stations Pacific - wide, including 3 near-field and 35 far-field stations covered by high-resolution inundation model grids, which are part of the test community models in Chile and part of the operational forecast system, respectively (Figs. 5 and 6). The inundation models for Chilean coastal locations have been developed as part of the ComMIT training exercise (Titov *et al.* 2011). As such, they have not been fully tested or scrutinized to the standards normally applied in the development of the operational tsunami flooding forecast models for the US coastal locations. The bathymetry and topography data for the Chilean model grids have been applied "as is" from the Global 30 Arc-Second Elevation (GTOPO30) global dataset (https://lta.cr.usgs.gov/GTOPO30) and Shuttle Radar Topography Mission (SRTM90) data respectively, without validation. Therefore, less precision results could be expected for these near-field models.

The data from the near-field Coquimbo and Valparaiso tide stations to the north and south of the epicenter show maximum positive wave amplitudes of 461 and 178 cm, respectively. High positive amplitudes were also observed at Hilo in Hawaii (81 cm), Pago Pago in Samoa (65 cm), Santa Barbara and Crescent City in California (34 and 30 cm, respectively), and Kingcove in Alaska (26 cm).

Figure 5 shows the computed maximum positive amplitude offshore for the 2015 Chile tsunami. The energy transported by a wave is directly proportional to the square of the wave height. High coastal amplitudes are in general correlated with high offshore amplitudes. The first wave of the 2015 Chile

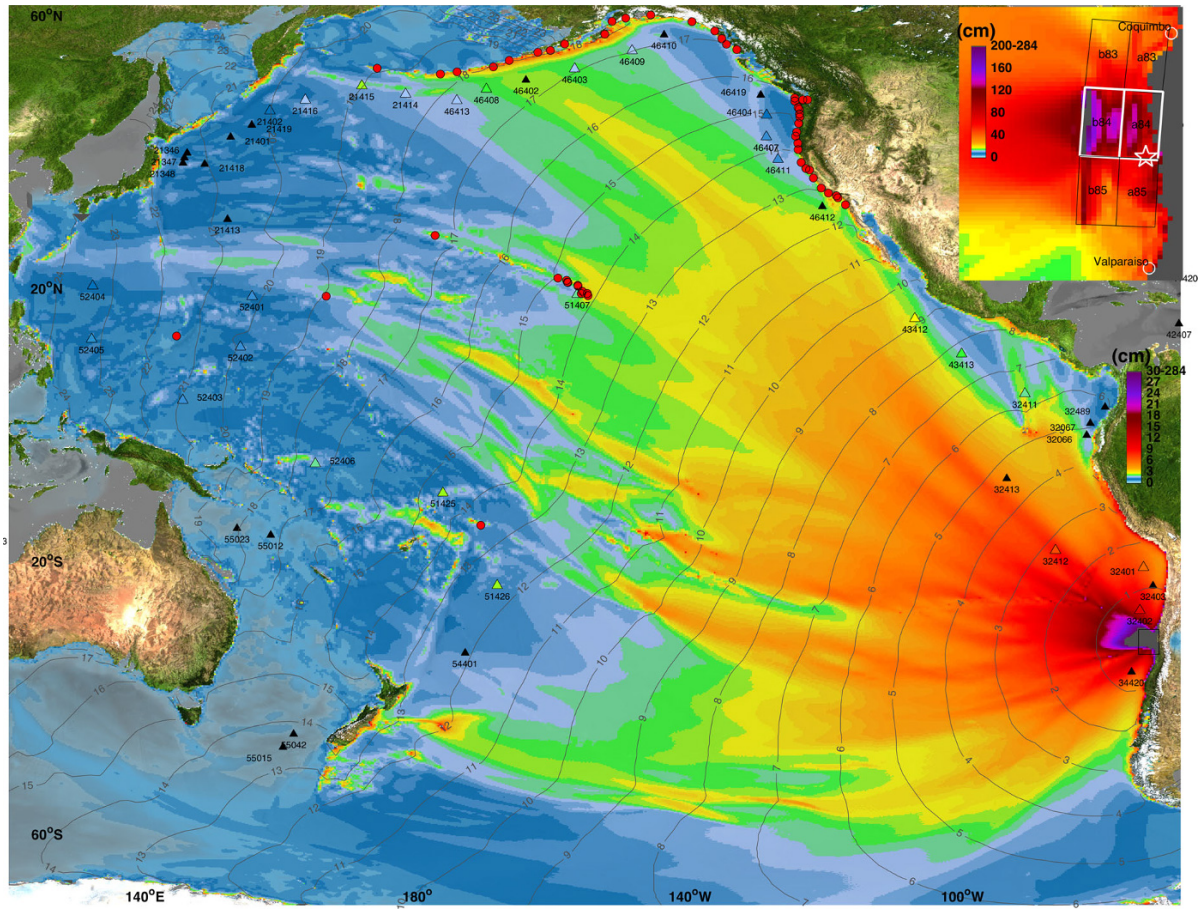

Figure 5
Energy propagation patterns guided by seafloor topography during the 2015 Chile tsunami. *Filled colors* show the modeled maximum positive amplitude in cm offshore during 30 h of wave propagation. *Contours* indicate computed tsunami arrival time in hours. *Triangles* indicate locations of tsunameters. *Colors* within the *triangles* represent the maximum observations at the tsunameters. The *triangles* filled in *black* indicate no observations were available at these stations. The *inset* shows fault geometry of the unit sources and close-up of the maximum positive amplitude in cm offshore. *Star* indicates the earthquake epicenter

tsunami arrived at the near-field coastlines with low tide (Fig. S3). At 23 min after the earthquake, the first wave arrived at the two near-field tide stations, Coquimbo and Valparaiso, with peaks of 93 and 119 cm, respectively. However, neither the first wave nor the second was the largest at the two stations (Fig. 7). At 1 h after the earthquake, a second wave of 432 cm crest was reported at Coquimbo tide station. At 1.5 h, the station recorded the largest crest of 461 cm as the third main wave. Similarly, at the Valparaiso tide station to the south of the epicenter, the 2nd and 3rd main waves with increasing crest of 147 and 178 cm arrived 1.2 and 1.8 h after the earthquake, respectively. At Talcahuano tide station, the first three main wave crests of 45, 124, and 120 cm recorded at 1.7, 3.2, and 4.7 h after the earthquake, respectively.

Figure 7 shows that all three tsunami sources obtained in real time are capable of producing good near-field model data comparisons for several consecutive tsunami wave amplitudes, following the general trend of observed tsunami time series for almost 6 h. Crude model bathymetry near sea-level gauges explains the time shift between modeled and observed waves peaks, since a mismatch between model and real bottom in a shallow bay would result in model errors in travel time and resonant frequencies. Nevertheless, good amplitude comparisons at

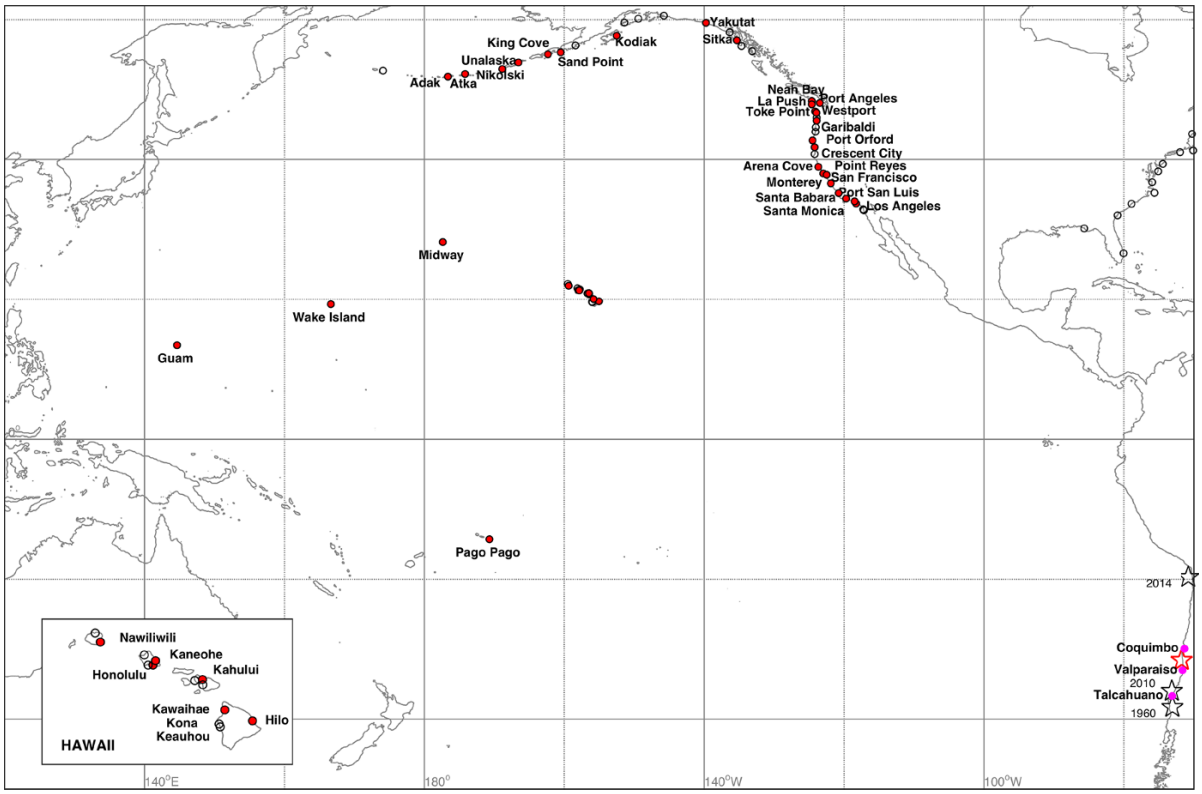

Figure 6
Locations of the coastal tide stations covered by high-resolution inundation model grids. *Pink circles* indicate the local tide stations in Chile, and *red circles* indicate the 35 coastal tide stations in the far-field. *Empty circles* are forecast sites with no tide gage data available for this event. *Red star* indicates the epicenter of the 2015 Chile earthquake, and the *black stars* indicate the earthquake locations for historical tsunamis in Chilean area

different coastal locations spread around the source imply that the quarter-wave source can provide accurate forecasts of amplitude and arrival time of the destructive waves for local sites, even with less than perfect model bathymetry. Maximum model run-up is even less sensitive to the source scenario. The Coquimbo model, covering all of Coquimbo Bay, shows maximum run-up from 6.8 to 6.9 m at about the same location in the south of the bay for all three model sources. The half-wave source produces the best prediction for the third wave, the maximum wave at the two closest tide stations (Fig. 7a, b). At Coquimbo station to the north of the epicenter, the early modeled arrival time from the quarter- and full-wave sources can be used to exclude unit source 83a from the main source area. In addition, at Valparaiso station to the south of the epicenter, the modeled early arrival time from the half- and full-wave sources can further eliminate unit source 85b. Thus, the main tsunami source area can be narrowed down to an area slightly over 100 km long and 100 km wide of unit sources 84a and 84b (Fig. 5 inset). It should be noted that each unit source in the propagation database has spatial resolution of 100 km in length and 50 km in width. To further refine the tsunami source with our inversion technique would require smaller unit sources with finer model grid resolution.

Figure 8 shows the forecast and observed amplitude time series up to 6 h after the tsunami arrived at 35 far-field coastal tide stations. For stations with good signal-to-noise ratio in the Hawaiian or Pacific Islands, the maximum wave appeared within the first 6 h. Hilo and Kahului stations again recorded the largest wave crests (81 and 57 cm, respectively) among the Hawaiian stations as they did for many past tsunamis (Tang *et al.* 2009, 2012). The two stations share two common geographical features. Both stations are located near the end of a bay, Hilo

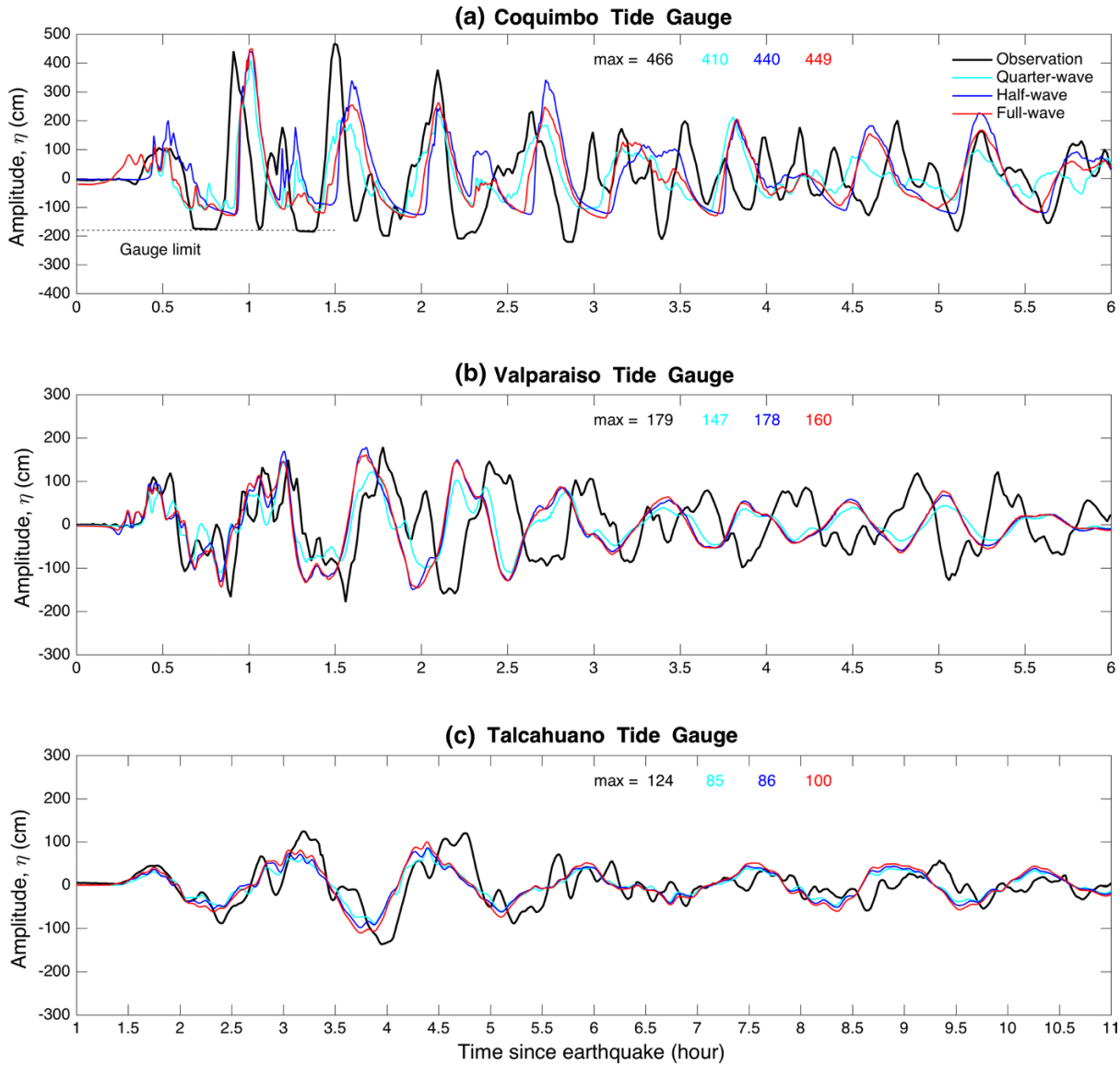

Figure 7
Observed and modeled time series of tsunami amplitude from the quarter-, half-, and full-wave sources at three local coastal tide stations in Chile for the 2015 Chile tsunami

and Kahului bays, respectively, with relatively gentle offshore slope (Fig. S2). These two features can enhance refraction focusing and local resonances regardless of the incoming direction of the tsunami source. Wavelet analyses of the observations at the two stations show a peak period of about 20–24 min for the incoming first positive half wave (Fig. S4). It quickly excited a strong resonant peak period of 16 min at the two sites, with a secondary peak period of 31 min. Those periods are consistent with the resonant periods reported in Tang *et al.* (2009) for the same sites. By contrast, the relatively flat coastal line and steep offshore slope for the Honolulu tide station make it record, repeatedly, the smallest tsunami amplitude (11 cm) among Hawaiian stations even though for this event it directly faces the incoming tsunami. Pago Pago tide station recorded the second largest maximum positive amplitude of 65 cm among the far-field stations, with a peak period of 18 min.

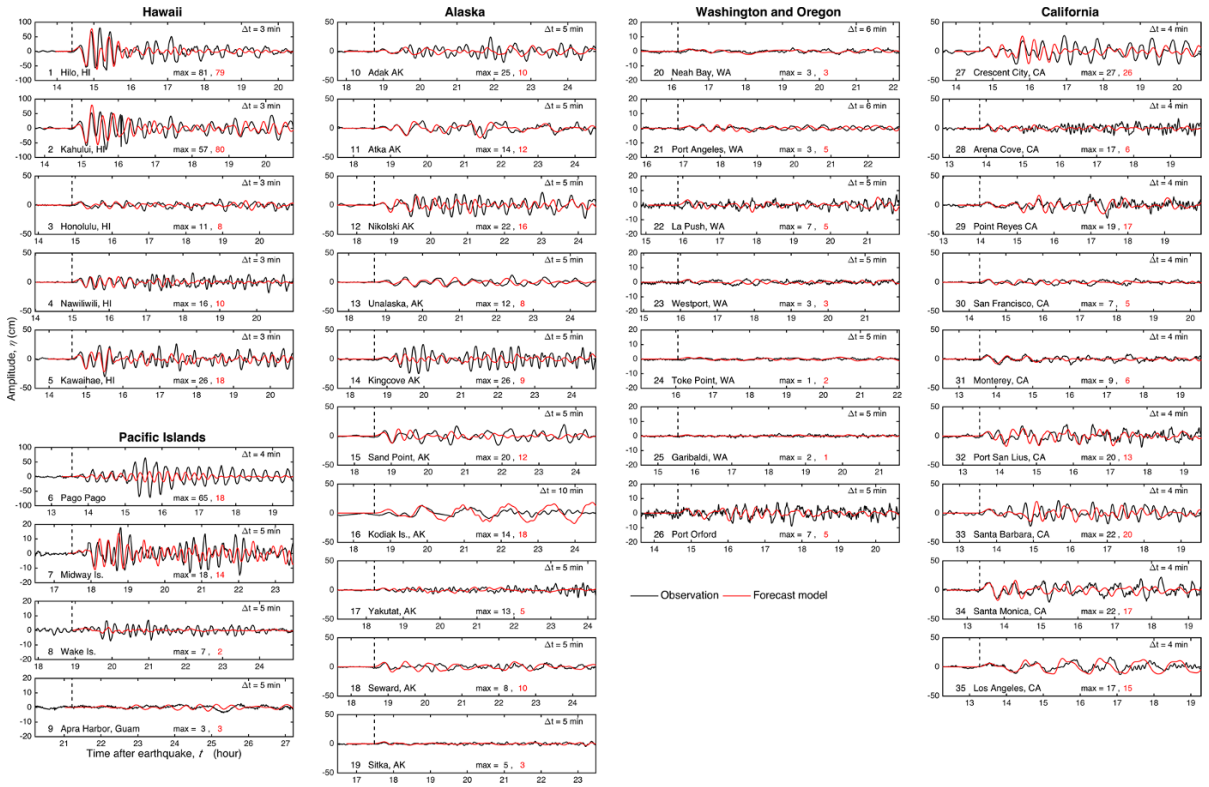

Figure 8
Forecast and observed time series of tsunami amplitude at 35 far-field coastal tide stations for the 2015 Chile tsunami. The *red lines* represent the model results obtained from the full-wave source

In general, from Alaska's Central to Eastern Aleutians, the maximum-recorded positive amplitude decreases gradually from 20+ cm at Adak station to 5 cm at the Sitka station (Fig. 8, panels 10–19). This pattern in coastal stations is correlated with the ray of relatively high-energy flux pointing to the Central Aleutian from the source (Fig. 5). The greater the distance from this ray, the smaller the recorded coastal amplitudes. This pattern is also evident from the coastal stations located within the states of Washington and Oregon, which recorded the smallest maximum positive amplitudes (no more than 7 cm during the first 6 h; Fig. 8, panels 20–26). For stations in California, the recorded maximum crests for the first 6 h are similar to those in the Central Aleutians: 7–27 cm (Fig. 8, panels 27–35). However, longer datasets show that the maximum wave arrived at the US West Coast about 26 h after the earthquake, which is about 12 h after the first wave (Fig. S5). The recorded maximum crests in the second 6 h increased to 11–34 cm for stations in California. Movie S1 and Fig. 1i reveal that this is correlated with the arrival time of the waves reflected from Eastern Aleutian, which have a nearly perpendicular incident angle to the US West Coasts.

To evaluate the performance of the forecast system for this tsunami, Fig. 9a compares the observations with modeled maximum crests from the three tsunami sources at the 38 coastal stations. The model error, $\text{err} = (\eta_{\max\ \text{model}} - \eta_{\max\ \text{obs}})/\eta_{\max\ \text{obs}}$, at each station for the first 6 h and up to 30 h are plotted in Fig. 9b, c, respectively. Among the stations with maximum crest greater than 50 cm (the warning threshold for dangerous tsunami waves), the Pago Pago forecast model produced the largest error. The maximum wave crest is 63–72 % underestimated with the three sources. However, at the nearest tsunameter station 51425, northwest of Apia, Samoa, all three sources show excellent forecast results in deep ocean, including the large late wave trains

(Fig. 2.19). This implies that the model discrepancy may stem from the setup of the model grids and/or the bathymetry of the Pago Pago forecast model, instead of the forecast source scenarios. The Pago Pago forecast model results are currently being investigated further to improve the forecast accuracy. Figure 9d, e further illustrates the improvement in model accuracy with increasing amplitudes. The average model accuracy is computed as $\frac{1}{N}\sum_{i=1}^{N}(1-|\mathrm{err}|)$, where N is the number of stations used.

Figure 9 shows higher accuracy for the first 6 h of modeled tsunami, when compared to maxima up to 30 h after earthquake. We attribute this partially due to the numerical dissipation caused by the coarse propagation model grid (Tang *et al.* 2012). It may underestimate waves trapped by the continental shelf over a long simulation time. In addition, the changing of incident angle by the wave reflected from the Eastern Aleutians, along with the trapped waves, can excite stronger resonance than the small, first incoming wave train for stations along the US West Coast.

Since the damaging impact usually happens within the first 6 h after tsunami arrival, this accuracy degradation has minimal impact on tsunami warning operations. Table 2 summarizes and quantifies the average accuracy for the first 6 h only. For the three sources, the averaged model accuracies for the maximum positive amplitudes at 38 coastal tide stations are 66, 69, and 69 % (or an average error of 9.0, 7.2, and 7.0 cm), respectively. We attribute the lower accuracy for sites with small amplitudes to the influence of ambient noise of the gauges that affects the signal-to-noise ratio. For six sites with observations greater than 50 cm, the average accuracies are 75, 76, and 76 %. Excellent model accuracies are also achieved for the three local sites, with 80, 88, and 89 % for the quarter-, half-, and full-wave sources, respectively. These are further improved to 86, 98, and 94 % for two local sites with observations greater than 150 cm.

The accuracy pattern of the 2015 Chile tsunami is similar to that of the 2011 Japan tsunami. Both events show higher accuracy for sites with larger amplitudes. For the 2011 Japan tsunami, the average forecast accuracy of the maximum crest at the 32 coastal tide stations is 68 %, or a 0.2 m average error (Tang *et al.* 2012). At the Crescent City, California and Kahului, Hawaii tide stations, which recorded the two largest maximum positive amplitudes of 2.5 and 2.1 m along the US West Coast and in Hawaii during the Japan tsunami, the accuracies are 98 and 95 %, respectively. Hence the system is capable of producing reliable forecast for flooding tsunami impacts not only in far field but also in near field.

5. *Implications for Fast and Reliable Forecast Application in the Near Field*

Our results suggest that tsunami energy can be reasonably estimated as early as the first quarter-wave recorded at a single tsunameter station for the 2015 Chile tsunami. This is due to the fact that the first quarter-wave of the tsunami signal carries the direct information—specifically, the location and wave energy of the tsunami source—while the later wave train contains reflection and refraction signals of the secondary tsunami interactions with bathymetry features and coastlines. As the result, the "quarter-wave source" (the inversion result of the quarter-wave tsunameter signal) is capable of providing accurate model forecasts for local coastal locations. The use of the "quarter-wave source" forecast for warning operations does, however, involves additional difficulties of carefully treating the tidal signal of the real-time data stream (Percival *et al.* 2015). With the first half-wave, the tidal-removal difficulties can be eliminated and the uncertainty of data inversion can be drastically reduced. Therefore, the "half-wave source" is sufficient to tune tsunami source parameters for accurate modeling of tsunami impact at any coastal sites, as implied by forecast analysis for this event. Using more data, such as the first full-wave, appears to provide only marginal improvements of forecast accuracy for this event.

Tang *et al.* (2012) show that the first wave recorded at two tsunameter stations in the vicinity of the 2011 Japan earthquake were sufficient to quantify the tsunami source energy of the highly destructive tsunami. The analysis of the 2015 Chile tsunami suggests further improvement of the forecast speed by using only the first quarter- or half-wave of

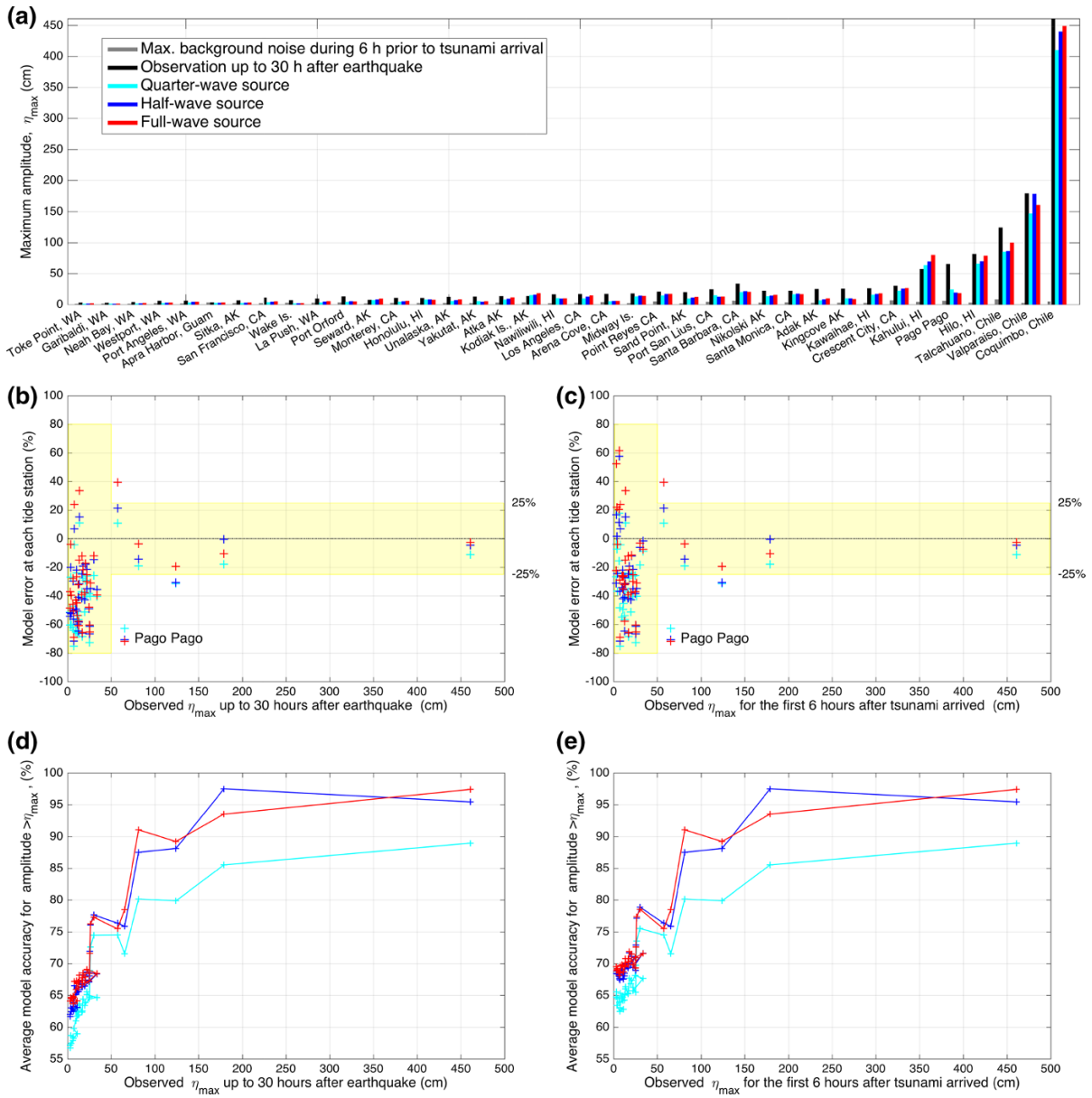

Figure 9

a Observed and modeled maximum positive amplitude from the quarter-, half-, and full-wave sources at 38 coastal tide stations for the 2015 Chile tsunami. **b**, **c** Model error at each station based on observations (**b**) during the first 30 h after earthquake and (**c**) during the first 6 h after tsunami arrival. **d**, **e** Average model accuracy for stations with observations greater than η_{max}

tsunameter recording. To test this hypothesis, we re-evaluated the 2011 Japan tsunami with model sources constrained by just the first quarter-wave recorded at the nearest tsunameter. We chose this event due to its high-quality survey data in the near field (The 2011 Tohoku Earthquake Tsunami Joint Survey Group 2011), and the availability of high-resolution model grids from Wei *et al.* (2013) for validation. The results are summarized in Fig. 10a–d. At 27 min after the 2011 Tohoku earthquake, the tsunami wave front reached the nearest tsunameter DART 21418. At 33 min, the station reported the first quarter-wave with maximum positive amplitude of 185 cm (Fig. 10b). The seven data points within 27 and

Table 2

Model accuracy at costal tide stations for the 2015 Chile tsunami

Coastal tide stations	No. of stations (*N*)	Average model accuracy (%) and error (cm)		
		Quarter-wave source	Half-wave source	Full-wave source
All	38	66 (9.0 cm)	69 (7.2 cm)	69 (7.0 cm)
Large signal - to - noise ratio (SNR[a] > 4)	22	66	70	71
Max obs. <50 cm	32	64	67	68
Max obs. >50 cm	6	75	76	76
Max obs. >80 cm	4	80	88	91
Max obs. >100 cm (near-field)	3	80	88	89
Max obs. >150 cm	2	86 (42 cm)	98 (11 cm)	94 (15 cm)

[a] SNR is computed as $S_{6h\ after\ tsunami}/S_{6h\ before\ tsunami}$, where *S* is the root mean square of the observations

33 min (1 min sample rate) were used to produce a quarter-wave source (39.3 × a26 + 39.3 × b26) (Fig. 10a, b). This quarter-wave source reproduced the flooding patterns in the most severely inundated coastal areas in Sendai, Japan (Fig. 10d). The estimated tsunami energy is 4.5×10^{15} J, which is 13–50 % greater than 3–4 × 10^{15} J obtained during the real-time assessment of this tsunami (Tang *et al.* 2012). Note that the first peak was reported as 164 cm in real time (Tang *et al.* 2012), which is 21 cm smaller than the current value. The discrepancy is due to different detiding algorithms involved in real-time assessment. Since then, the detiding algorithm for use in real time has been improved (Percival *et al.* 2015).

The "quarter-wave source" was available 23 and 30 min earlier than the "full-wave source" for the 2011 Japan and 2015 Chile tsunamis, respectively. These 23–30 min can be a critical time difference for the local forecast and warning operations.

Note that the quarter-wave source for the 2015 Chile tsunami produced much better comparisons at the second tsunameter (Fig. 2.2) than during the 2011 Japan tsunami (Fig. 10c). The fact that the first-detector station of the Chile event, DART 32402, is located off the main beam of tsunami propagation energy to the side of the tsunami source is, in fact, advantageous for the tsunami source inversion purposes, which may be contrary to intuition. Figure 11a shows 4–14 min differences in the peak travel time (mainly due to the differences in travel distance) for unit sources within three columns (83–85) for the Chile event, while the Japan tsunami only shows 0–3 min differences for four columns (24–27) of unit sources (Fig. 11b). The significant differences in travel time/distance from the adjacent unit sources to the Chile station can reduce ambiguity of source unit location and, therefore, locate the tsunami origin more precisely.

Our results indicate that the earliest estimate of tsunami energy and local forecasts can start with the first quarter-wave recorded at the nearest tsunameter regardless of the orientation of the station to the source. However, when the nearest tsunameter is at the optimum orientation to the source, the half-wave data from a single near-field tsunameter may provide sufficient accuracy for forecast purpose, as in the case of the 2015 Chile tsunami. Otherwise, data from another tsunameter with a better orientation relative to the source may be required to refine the forecasts, as in the case of the 2011 Japan tsunami.

6. Conclusion and Future Work

The 2015 Chile tsunami provided a unique opportunity to quantify the minimum tsunameter data for the earliest possible tsunami forecast. The real-time assessment of this event implies that the tsunameter sea level data of just the first quarter wave period can provide a reliable tsunami energy estimate and coastal forecast that would be useful for local warning operations. The analysis of the 2011 Japan tsunami data further confirmed this conclusion. In addition, tsunameter data of the first half-wave period were sufficient to accurately define the two most important characteristics of a tsunami source: the location of origin and the tsunami energy for the 2015

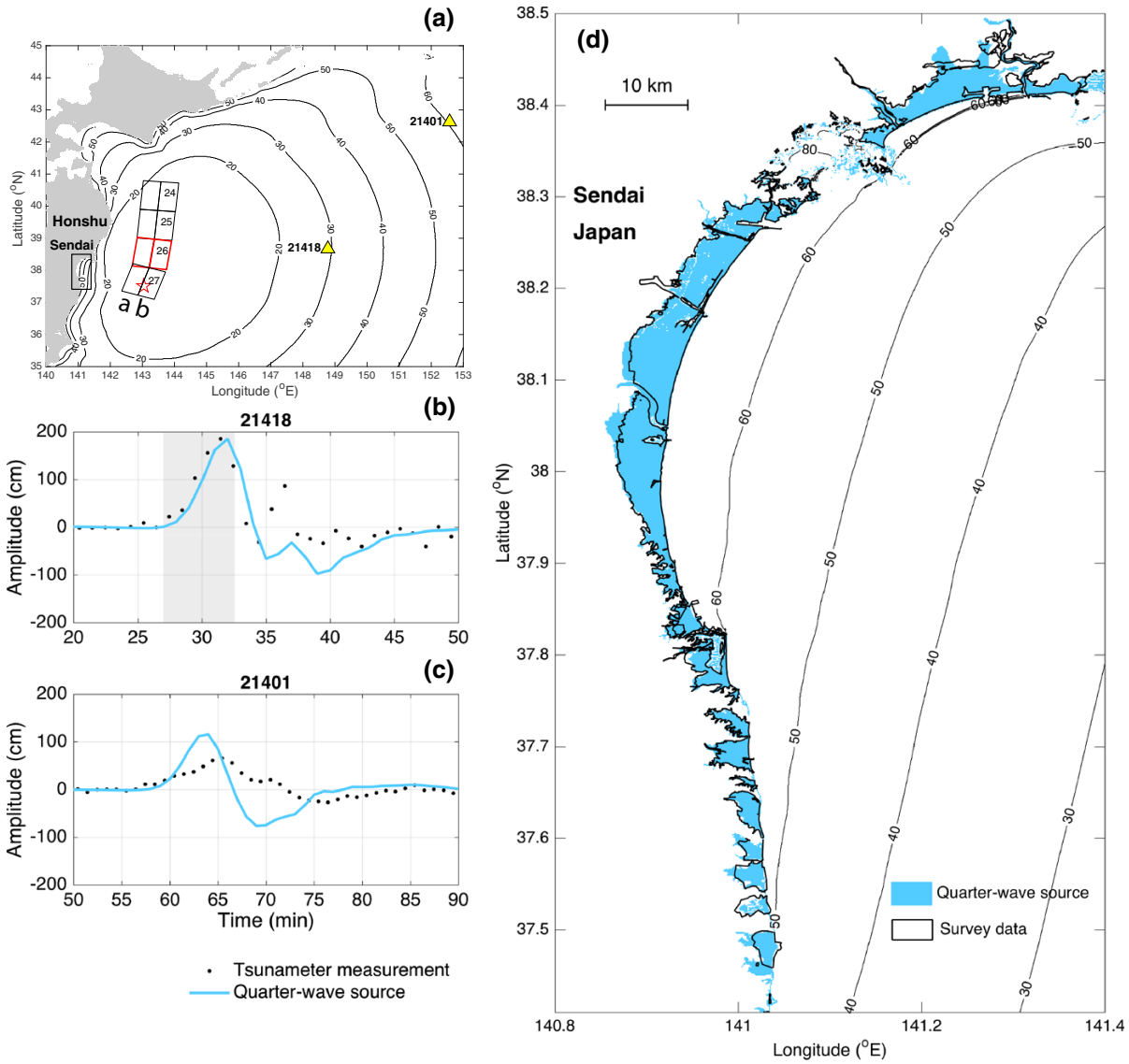

Figure 10

a Locations of the two nearest tsunameter stations (*yellow triangles*), pre-computed unit sources (*black* and *red rectangles*) near the epicenter of the 2011 Japan earthquake (*red star*), and Sendai, Japan. **b**, **c** Measurements and model time series at the two tsunameters. Data within the inversion time window in (**b**), 27–33 min after the earthquake (in *grey*) were used to generate a quarter-wave source. **d** The quarter-wave source model inundation area (*blue*) compared with measured tsunami flooding areas in Sendai. *Contours* in **a** and **d** indicate modeled tsunami arrival time in minutes

Chile tsunami. The position of the nearest tsunameter for the Chile tsunami is to the side of the tsunami source. The relatively significant differences in travel time/distance from the adjacent unit sources to the tsunameter reduce the ambiguity of source unit location and, therefore, locate the tsunami origin more precisely.

Coastal sea level records of the tsunami at Coquimbo and Valparaiso tide stations showed that the destructive tsunami flooding arrived at both locations as the 2nd wave, about 1 h after the earthquake, while the third wave, 1.5 h after the earthquake, was the largest. These data, coupled with our modeling analysis, imply that accurate model

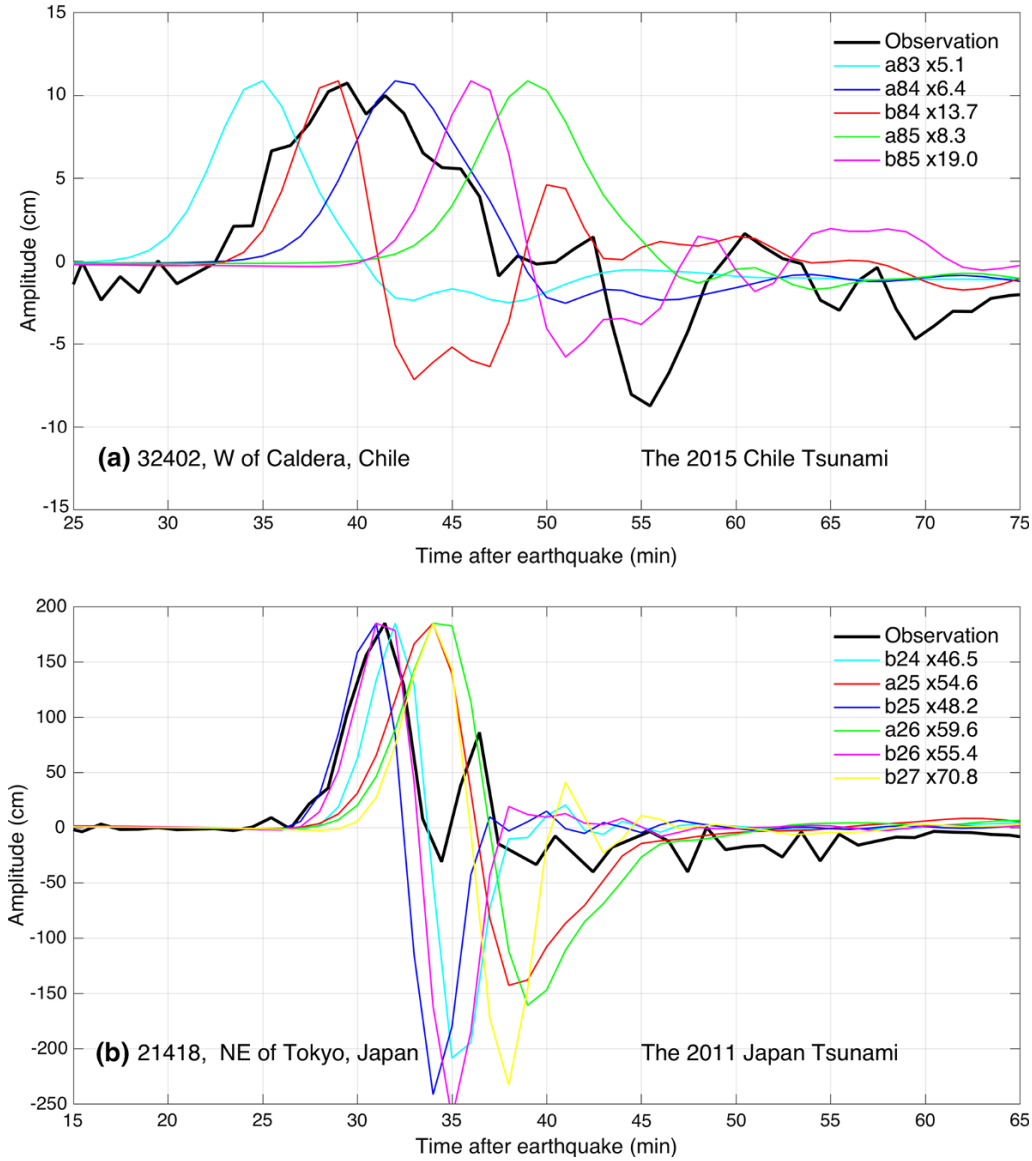

Figure 11

a Significant differences in travel time from the unit sources to the nearest tsunameter when the station is located off the main beam of tsunami propagation energy (to the side of the tsunami source) for the 2015 Chile tsunami. **b** Similar travel times are observed when the nearest tsunameter is located in the main energy beam (i.e. the propagation path from the source to the station is nearly perpendicular to the trench) for the 2011 Japan tsunami. The time series of each unit source is scaled to the observed maximum positive amplitude by multiplying the corresponding coefficient in the legend

forecasting of tsunami flooding could potentially provide valuable information before destructive waves arrive not only in the far-field, but also for many near-field communities, if tsunameter data are available sooner.

Along with active and aggressive education measures for self-evacuation, fast and accurate forecasts of flooding may provide better guidance for evacuation decisions that will save lives and provide focus for real-time tsunami mitigation measures. As part of the continuing effort to improve the national warning system and as a valuable contribution to the international tsunami warning system, the Hydrographic and Oceanographic Service of the Chilean

Navy (SHOA) deployed two experimental new-generation DART 4G tsunameters, as a joint pilot project with NOAA to test new local tsunami forecast capabilities. The deployment was carefully organized and planned in the NOAA-SHOA agreement crafted more than a year ago. The planned deployment date was set on 23 September 2015, exactly 1 week after the tsunami of the 16 September. The new instrument (and PMEL/SHOA engineering team) survived the tsunami inundation onshore at the port of Valparaiso, and it was successfully deployed offshore as planned. While the instrument missed this first opportunity, the test deployment will certainly provide data in the near future to assess the local forecast capability based on reduced tsunami detection time. These 4G tsunameters are equipped with a new generation of pressure sensor, named nano-resolution pressure sensors, which can detect and separate a tsunami signal out of the earthquake shaking noise (Paros *et al.* 2011). Therefore, they could be deployed much closer to potential tsunami sources and could record tsunami waves right at the time of origin, saving valuable time for providing forecast to the local coastal population. The testing of this new technology and modeling for near-field forecasting with the past Chile tsunamis will be presented in a more specific, forthcoming study.

Acknowledgments

The authors thank Dr. Donald W. Denbo for obtaining the quarter-wave source during real-time assessment of the 2015 Chile tsunami; the reviewers for their valuable comments that enhanced the paper; NCTR members for discussion and contributions; Sandra Bigley for comments and edits; Stuart A. Weinstein, Hydrographic and Oceanographic Service of the Chilean Navy (SHOA), and National Ocean Service Center for Operational Oceanographic Products and Services (NOS/CO-OPS) for water level data; and National Data Buoy Center (NDBC) for tsunameter data. This research is funded by the NOAA Center for Tsunami Research, PMEL contribution # 4394. This publication is partially funded by the Joint Institute for the Study of the Atmosphere and Ocean (JISAO) under NOAA Cooperative Agreement NA10OAR4320148, Contribution No. 2470.

References

Bernard, E., Y. Wei, L. Tang, and V.V. Titov (2014). *Impact of Near-Field, Deep-Ocean Tsunami Observations on Forecasting the 7 December 2012 Japanese Tsunami*. Pure and Appl. Geophys., *171*(12), doi:10.1007/s00024-013-0720-8, 3483–3491.

Bernard, E., and Titov,V.V. (2015). *Evolution of tsunami warning systems and products*. Philos. Trans. R. Soc. Lond. A, *373*(2053), 20140371, doi:10.1098/rsta.2014.0371.

Bonnefoy, P. and Romero, S. (2015). In Chile, Earthquake Forces One Million to Evacuate. The New York Times, http://www.nytimes.com/2015/09/17/world/americas/chile-earthquake.html?_r=0.

Fujii, Y. and Satake, K. (2013). *Slip distribution and seismic moment of the 2010 and 1960 Chilean earthquakes inferred from tsunami waveforms and coastal geodetic data*, Pure. Appl. Geophys*., 170*, 1493–1509, doi:10.1007/s00024-012-0524-2.2013.

Fritz, H.M., Petroff, C.M., Catalán, P., Cienfuegos, R., Winckler, P., Kalligeris, N., Weiss, R., Barrientos, S.E., Meneses, G., Valderas-Bermejo, C., Ebeling, C., Papadopoulos, A., Contreras, M., Almar, R., Dominguez, J.C., and Synolakis, C.E. (2011). *Field Survey of the 27 February 2010 Chile Tsunami*. Pure Appl. Geophys., *168*(11):1989–2010, doi:10.1007/s00024-011-0283-5.

Gica, E., Spillane, M., Titov, V.V., Chamberlin, C. and Newman, J.C. (2008). Development of the forecast propagation database for NOAA's Short-term Inundation Forecast for Tsunamis (SIFT), NOAA Tech. Memo. OAR PMEL-139, 89 pp, Gov. Print. Off., Seattle, Wash.

González, F.I., Bernard, E.N., Meinig, C., Eble, M., Mofjeld, H.O. and Stalin, S. (2005). *The NTHMP tsunameter network*, Nat. Hazards, *35* (1), 25–39.

Gusiakov, V. K. (1978). Static displacement on the surface of an elastic space, in Ill-Posed Problems of Mathematical Physics and Interpretation of Geophysical Data (in Russian), pp. 23–51, Comput. Cent. of Sov. Acad. of Sci., Novosibirsk, Russia.

Kanamori, H. (1977). *The energy release in great earthquakes*, J. Geophys. Res., *82* (20), 2981–2987.

Liu, P. L.-F. (2009). Tsunami modeling: Propagation, in The Sea, Tsunamis Ch. 3 15 edited by E. Bernard *et al.* 295-320, Harvard Univ. Press, Cambridge, MA.

Mei, C.C., M. Tiassnie, and D.Yue (2005). Theory and Applications of Ocean Surface Waves, Part 1: Linear Aspects. World Scientific.

Meinig, C., Stalin, S.E., Nakamura, A.I., González, F. and Milburn, H.G. (2005). Technology Developments in Real-Time Tsunami Measuring, Monitoring and Forecasting, In Oceans 2005 MTS/IEEE, 19–23 September 2005, Washington, D.C.

Milburn, H.B., A.I. Nakamura, and F.I. Gonzalez (1996). Real-time tsunami reporting from the deep ocean. Proceedings of the Oceans 96 MTS/IEEE Conference, 23–26 September 1996, Fort Lauderdale, FL, 390–394.

Onemi, (2015). Monitoreo por sismo de mayor intensidad. (In Spanish) [Available at: http://www.onemi.cl/alerta/se-declara-alerta-roja-por-sismo-de-mayor-intensidad-y-alarma-de-tsunami/]

Okada, Y. (1985). *Surface deformation due to shear and tensile faults in a half space*, Bull. Seism. Soc. Am., *75*, 1135–1154.

Paros, J., Bernard, E., Delaney, J., Meinig, C., Spillane, M., Migliacio, P., Tang, L., Chadwick, W., Schaad, T. and Stalin, S. (2011). Breakthrough underwater technology holds promise for improved local tsunami warnings, In Symposium for Underwater Technology 11/IEEE.

Percival, D.B., Denbo, D.W., Eble, M.C., Gica, E., Mofjeld, H.O., Spillane, M.C., Tang, L. and Titov, V.V. (2011). *Extraction of tsunami source coefficients* via *inversion of DART® buoy data*, Nat. Hazards, *58*(1), doi: 10.1007/s11069-010-9688-1, 567–590.

Percival, D.B., Denbo, D.W., Eblé, M.C., Gica, E., Huang, P.Y., Mofjeld, H.O., Spillane, M.C., Titov, V.V. and Tolkova, E.I. (2015). *Detiding DART® buoy data for real-time extraction of source coefficients for operational tsunami forecasting*. Published online, Pure Appl. Geophys., June 2015, Vol. *172*, Issue 6, pp 1653–1678, doi:10.1007/s00024-014-0962-0.

Spillane, M.C., Gica, E., Titov, V.V. and Mofjeld, H.O. (2008). Tsunameter network design for the US DART® arrays in the Pacific and Atlantic Oceans, Tech. Memo, OAR PMEL-143, 165 pp., Gov. Print. Off., Seattle, Wash.

Synolakis, C., Bernard, E.N., Titov, V.V., Kanoglu, U. and Gonzalez F. (2008). *Validation and verification of tsunami numerical models*, Pure Appl. Geophys., *165*(11–12), 2197–2228, doi:10.1007/s00024-004-0427-y.

Tang, L., Titov, V.V., Wei, Y., Mofjeld, H.O., Spillane, M., Arcas, D., Bernard, E.N., Chamberlin, C.D., Gica, E. and Newman, J. (2008). *Tsunami forecast analysis for the May 2006 Tonga tsunami*, J. Geophys. Res., *113*, C12015, doi: 10.1029/2008JC004922.

Tang, L., Titov, V.V. and Chamberlin, C.D. (2009). *Development, testing, and applications of site-specific tsunami inundation models for real-time forecasting*, J. Geophys. Res., *114*, C12025, doi:10.1029/2009JC005476.

Tang, L., Titov, V.V., Bernard, E.N., Wei, Y., Chamberlin, C.D, Newman, J.C., Mofjeld, H., Arcas, D., Eble, M., Moore, C., Uslu, B., Pells, C., Spillane, M.C., Wright, L.M. and Gica, E. (2012). *Direct energy estimation of the 2011 Japan tsunami using deep-ocean pressure measurements,* J. Geophys. Res., *117*, C08008, doi:10.1029/2011JC007635.

The 2011 Tohoku Earthquake Tsunami Joint Survey Group (2011). Post-tsunami field survey of the 2011 Tohoku earthquake tsunami, XXV IUGG Assembly, Melbourne, Australia.

Titov, V.V., U. Kanoglu and C.S. Synolakis, (2015), Development of a Model for Real-time Tsunami Forecasting: from VTCS to MOST, Journal of Waterway, Port, Coastal and Ocean Engineering, accepted.

Titov, V.V. and Synolakis, C.S. (1998). *Numerical modeling of tidal wave runup*. Journal of Waterway, Port, Coastal and Ocean Engineering *124*(4), 157–171.

Titov, V.V. and Gonzalez, F.I. (1997). Implementation and testing of the Method of Splitting Tsunami (MOST) model, NOAA Tech. Memo. ERL PMEL-112, Pacific Marine Environmental Laboratory, Seattle, WA.

Titov, V. V., Mofjeld, H. O., Gonzalez, F. I. and Newman, J.C. (1999). Offshore forecasting of Alaska-Aleutian subduction zone tsunamis in Hawaii, Tech. Memo. ERL PMEL-114, 22 pp., Gov. Print. Off., Seattle, Wash.

Titov, V.V., Rabinovich, A.B., Mofjeld, H.O., Thomson, R.E. and González, F.I. (2005). *The global reach of the 26 December 2004 Sumatra Tsunami*. Science, *309*(5743), 2045–2048.

Titov, V.V. (2009). Tsunami forecasting, in The Sea, Tsunamis Ch. 12 15, edited by E.N. Bernard, Harvard Univ. Press, Cambridge, MA.

Titov, V.V, Moore, C.W., Greenslade, D.J.M., Pattiaratchi, C., Badal, R., Synolakis, C.E. and Kânoğlu, U. (2011). *A New Tool for Inundation Modeling: Community Modeling Interface for Tsunamis (ComMIT),* Pure and Appl. Geophys. doi: 10.1007/s00024-011-0292-4.

Titov V.V. and Tang, L. (2011). Estimating tsunami magnitude in real time using tsunameter data, the XXV IUGG General Assembly, Melbourne Australia, 28 June–7 July, 2011.

Titov V.V. and Tang, L. (2015). Tsunami Magnitude as Measure of Potential Impact, IUGG-4515, the 26th IUGG General Assembly, Prague, Czech Republic, June 22–July 2, 2015.

Wei, Y., Bernard, E.N., Tang, L., Weiss, R., Titov, V.V., Moore, C., Spillane, M., Hopkins, M. and Kânoğlu, U. (2008), *Real-time experimental forecast of the Peruvian tsunami of August 2007 for US coastlines*, Geophys. Res. Lett., *35*, L04609, doi: 10.1029/2007GL032250.

Wei, Y., Chamberlin, C.D., Titov, V.V. and Tang, L. (2013). *Modeling of the 2011 Japan tsunami: lessons for near-field tsunami forecast*, Pure Appl. Geophys., *170*(6–8), doi: 10.1007/s00024-012-0519-z, 1309–1331.

Ye, L., Lay, T., Kanamori, H. and Koper K.D. (2015). *Rapidly estimated seismic source parameters for the 16 september 2015 Illapel, Chile Mw 8.3 Earthquake*, Pure Appl. Geophys., doi:10.1007/s00024-015-1202-y

(Received October 20, 2015, revised December 2, 2015, accepted December 7, 2015, Published online January 30, 2016)